PANORAMIC PHOTOGRAPHY ANALYSIS APOLLO 15

William C. Kinney

Itek Corporation, Massachusetts

Introduction

This paper is a two-stage study of the photographic aspects of the Apollo optical bar camera. The first part, prepared and presented in advance of the flight of Apollo 15, deals with the analysis of the lunar surface characteristics; defines the film, filter, and exposure for optimum camera performance; and investigates lunar object detection. These studies led to the choice of the photographic camera parameters incorporated in the mission. The second part is an analysis of the quality of the optical bar photography with particular attention given to the correlation between the predictions of part one and the actual results derived from measurements of the imagery. These findings are presented (1) to demonstrate the image quality of the photography and (2) to substantiate the value of photographic predictions as a means to ensure optimum camera performance.

PART I

APOLLO OPTICAL BAR CAMERA PHOTOGRAPHIC SYSTEM ANALYSIS AND LUNAR OBJECT DETECTION STUDY

Introduction

The acquisition of lunar photography with the Itek optical bar camera is a complex problem requiring thorough analysis and a congruous integration of several system parameters. These parameters are the lunar surface luminance, the flight film and filter, and the film processing specifications. An analysis of any one factor will not provide adequate insight into the quality of the lunar surface imagery. Indeed, the optical bar photographic system can be optimized only if all the associated parameters are treated as a complex array where each is adjusted as a function of all the others.

Lunar object detection and the identification of lunar module landing hazards is a prime objective of the optical bar Apollo missions. The qualitative definition of this capability is dependent not only on the above mentioned parameters, but also on optical characteristics of the lenses and the associated camera dynamics. Defining the system image quality potential by translation from standard three-bar resolution measurements to ground resolved distance predictions is misleading, and in most cases totally invalid.

This paper is intended to provide insight into the capability and potential of the optical bar imaging system. It is based on evidence acquired from calculations concerning the lunar surface. The surface object characteristics considered are luminance, size, and shape, since all three factors contribute to the object's potential detectability.

The paper is divided into two principal parts: lunar surface luminance, exposure, and system resolution; and lunar object detection. A basic discussion of the general concept and a detailed account of its specific application to the optical bar camera are presented. In some cases, the results of this study are only preliminary and should be considered as background for future research.

Lunar Surface Luminance, Exposure, and System Resolution

Lunar Surface Luminance

The amount of light reflected from a surface,

i.e., luminance, is dependent on three factors:

1. The amount of light incident on the surface, i.e., illuminance
2. The spectral reflectance of the surface
3. The reflection characteristics of the surface.

Illuminance. Illuminance, or illumination, is defined as the luminous flux incident on a surface per unit area. It is generally measured in terms of meter-candles or foot-candles, the latter being equal to 1 lumen per square foot.

The illuminance of the moon, because of the lack of atmosphere, is solely dependent on the intensity of the sun. It is constant for all solar altitudes and is approximately 13,000 ft-c. Its spectral composition or color temperature is approximately 5,800 °K.

Spectral Reflectance. The spectral reflectance of the surface material is dependent primarily on its composition. Spectroscopic examination of surface fines recovered from Tranquility Base, Apollo 11, have a spectral reflectance as shown in Fig. 1. Other materials such as crystalline rocks and breccias have similar curve shapes, with the only change being variations in the percent reflection.

The spectral characteristics of the surface-reflected light, i.e., surface luminance, is an important consideration when making calculations concerning the total system sensitivity. Combining the spectral distribution of the illumination (sun) and the spectral reflection of the surface materials shows the spectral composition of the luminance (reflected light) to be between 4,700 and 4,900 °K.

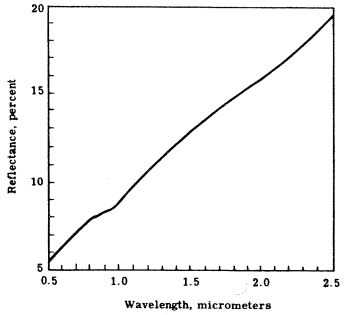

Fig. 1 — Spectral reflectance curve of surface fines from Apollo 11 lunar samples

Reflection Characteristics. Reflecting surfaces are generally classified as specular, diffuse, and specular-diffuse. If the light reflected from a surface is such that the angle of reflection is equal to the angle of incidence, the surface is said to be specular, e.g., a front coated mirror. If the amount of reflected light is equal in all directions and is independent of the angle of incidence, the surface is said to be diffuse or Lambertian. This condition is approximated by the reflection characteristics of magnesium oxide. A specular-diffuse surface is obviously a combination of the two. Most reflecting surfaces fall into this classification.

The reflection characteristics of the earth and moon are shown in Fig. 2. The earth is specular-diffuse; it is primarily diffuse with a peak along the line of specular reflection and a minor peak in the direction of the incident light. The reflective nature of the lunar surface, however, is not only different from that of the earth, but peculiar to most reflecting surfaces. Virtually all the light is reflected back in the direction of incidence. There is a rapid reduction in intensity as the angle of reflectance departs from the angle of incidence.

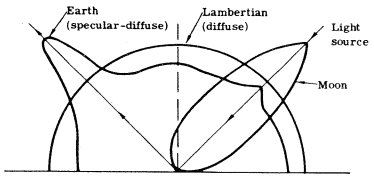

Fig. 2 — Reflection characteristics of earth and moon

The amount of light reflected back from the lunar surface (luminance) for all conditions of illuminance and viewing can be expressed by only two angles:

α—the phase angle, the angle between the incidence and viewing vectors

τ—the angle between the viewing vector and the normal to the surface slope when projected into the phase plane.

The angles and vectors along with the sign convention are illustrated in Fig. 3. Note that τ is positive only if the viewing vector is between the surface normal and incidence vector.

The relationships between the amount of reflected light and the angles α and τ are described by a series of functions derived from data obtained by Fedorets. These functions are shown in Fig. 4. The photometric function, ϕ, determines the surface luminance by the relationship

$$\beta = \phi \rho E_S \qquad (1)$$

where β = luminance (foot-lamberts)
ϕ = Fedorets' photometric function
ρ = surface albedo
E_S = solar illuminance = 13,000 ft-c

The lunar surface albedo describes the percentage of light reflection independent of illuminance surface geometry. It is determined primarily by the composition of the surface fines and can vary from 6 to 18% depending on the presence of such elements as iron and titanium. An albedo of 7% is representative of lunar maria.

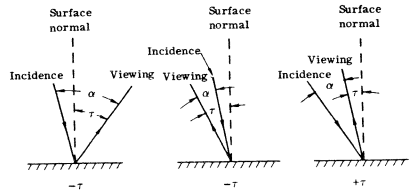

Fig. 3 — Photometric angles

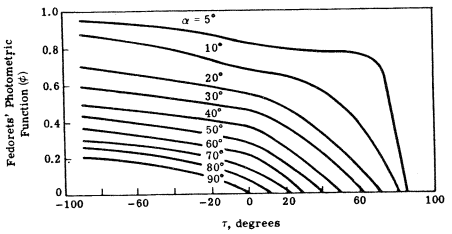

Fig. 4 — Fedorets' photometric curves

Lunar Luminance and Camera Geometry. It is possible to describe the changes in surface luminance as a function of the geometry of the optical bar camera. Since the camera is pan scanning and stereo recording, it is necessary to make some assumptions to simplify the task to bring it into the scope of this paper. First, since the surface luminance will vary between the fore and aft looking modes as a function of solar altitude, two sets of functions are necessary to provide an adequate description of the luminance distribution. Second, the luminance change will be determined at the center of the format. Third, the surface slopes will vary such that the normal to the surface will always be located in the phase plane. The positive slopes represent those surfaces facing the sun and the negative slopes those surfaces away from the sun. Fourth, an albedo of 9% is assumed, the one considered to be predominant over the surface.

The changes in surface luminance as a function of solar altitude and surface slope are shown in Figs. 5 and 6 for the fore and aft looking camera conditions.* From a cursory examination of Lunar Orbiter and Apollo photography it was obvious that there seldom were surface slopes greater than 30°. Limit lines representing ±30° slope are therefore indicated on the figures, and it is this range of luminances that are used to generate the curves of Fig. 7. The mean luminance indicated in Fig. 7 is the predominant one that will be perceived by the optical bar light sensor. It is therefore not derived mathematically but rather is the luminance associated with the predominant surface slope, i.e., the 0° slope.

The mean luminance and luminance range as a function of solar altitude are used as the basis for determining the exposure criteria.

Exposure

Exposure is defined as the quantity of light received by the photographic emulsion. It is

*The curves are labeled with the assumption that the camera is traveling from the terminator (0° solar altitude) to subsolar (90° solar altitude). The luminance change associated with a camera movement from subsolar to terminator would merely require a reversal of the fore and aft look conditions.

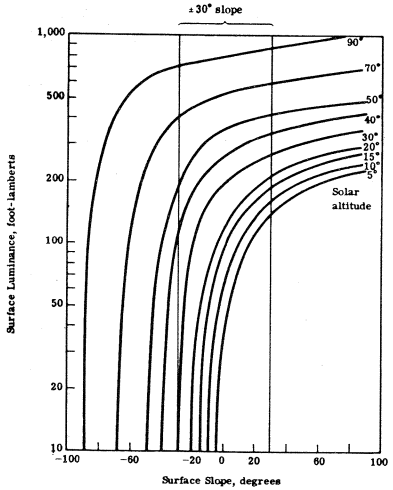

Fig. 5 — Surface slope versus surface luminance for various solar altitudes (forward looking camera, 9% albedo)

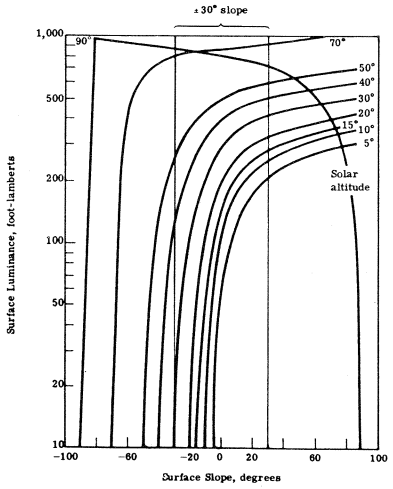

Fig. 6 — Surface slope versus surface luminance for various solar altitudes (aft looking camera, 9% albedo)

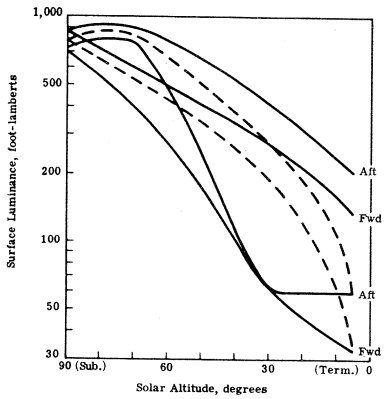

Fig. 7 — Solar altitude versus surface luminance (scene slope increment = 5°, slope limits = ±30°)

the product of the rate at which light falls on the emulsion surface and the time during which the light is received. It is calculated by

$$E = It \qquad (2)$$

where E = exposure (usually expressed in meter-candle-seconds)
I = illuminance (usually in meter-candles)
t = time (usually in seconds)

The exposure received by the photographic emulsion is converted to a visual density usually by chemical development. The relationship of the density to the exposure is customarily presented in graphical form with the density plotted as a function of the logarithm of exposure. This function is generally referred to as a D–log E curve, an H&D curve (named after Hurter and Driffield, who first employed such curves), or a characteristic curve. A typical H&D curve for Eastman Kodak type 3414 film is shown in Fig. 8.

Emulsion Speed. The efficiency of an emulsion to yield density as a function of exposure is termed the photographic emulsion speed and is defined as the reciprocal of the exposure required to produce a given density.

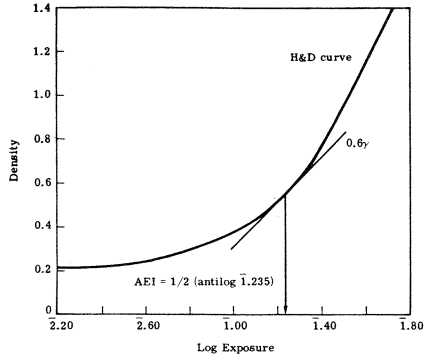

Fig. 8 — H&D curve for 3414 film (Fultron processor, MX-819-1 developer, AEI = 2.9, fog = 0.20, gamma = 1.96)

The speed of an emulsion is dependent on several factors:

1. The chemical composition of the emulsion
2. The size frequency distribution of the silver halide grains
3. The spectral sensitivity of the emulsion.

It is also somewhat sensitive to the type of development and the spectral distribution of the illumination. A typical speed index for aerial films is the aerial exposure index (AEI) defined by the relationship

$$AEI = 1/2E \qquad (3)$$

where E is the exposure required to produce a density on the H&D curve corresponding to a position where the gradient is 0.6 of the gamma.

Exposure Determination. When a photographic film is exposed in a camera system, the simple relationship of Eq. 2 is expanded to encompass the transmission characteristics of the optical system. The expanded equation is

$$E = \frac{2.7t\beta T_l}{(f/no.)^2 F} \qquad (4)$$

where t = exposure time (seconds)
β = scene luminance from Eq. 1 (foot-lamberts)
T_l = lens transmission (percent)
f/no. = lens f/number
F = filter factor

This relationship makes it possible to determine the exposure time required to produce a given density by considering the film H&D curve and the level of luminance.

Applying the previously discussed exposure considerations to the optical bar camera conditions allows for a concise statement of the problem: What is the minimum exposure time necessary to record the scene luminance ranges at the various solar altitudes?

It is desirable to minimize the exposure time since it is directly related to image smear, a major contributor to the degradation of system resolution. The image smear is computed from

$$b = \dot{b}t \qquad (5)$$

where b = smear (micrometers)
$\dot{b}$ = system smear (micrometers per millisecond)
t = exposure time (milliseconds)

The amount of system smear is shown in Table 1.

Table 1 — Smear Budget at Center of Format

Source	Smear Rate, μm/msec: Along Track	Cross Track
Film synchronization	—	0.4000
2% FMC error	0.170	—
Vehicle roll of 0.018°/sec	—	0.192
Vehicle pitch of 0.0042°/sec	—	—
Total	0.170	0.592

The exposure time for a given scene luminance can be reduced by employing several techniques, most notably either by changing the camera filter or by using a faster film.

A wider band filter will transmit a greater percentage of the reflected lunar luminance, thereby permitting shorter exposure times. For example, converting from a Wratten 23A filter to a Wratten 12 filter will increase the system transmission by $1\frac{1}{2}$ to 2 times, depending on the spectral sensitivity of the camera film. The only difficulty in making this

alteration is that the optical bar Petzval lens is designed for use with a Wratten 23A filter. Consequently, as the cutoff frequency is reduced by employing other filters, e.g., the W-12, the lens chromatic aberrations increase, resulting in lower resolution performance. Tradeoff studies between smear as a function of camera filter and chromatic aberration are presented in the next section.

The use of a faster film, e.g., 3400 instead of 3414, will effectively reduce the required exposure time, but, as with the filter change, will result in a sacrifice in system resolution. This lower resolution is manifested by the film's increased granularity, a consequence of its higher speed.

Midrange Exposure Point. The fundamental problem is not only to optimize the film-filter-processing parameters as a function of maximum resolution, but also to determine the relationship between the scene's luminance ranges at various solar altitudes and the resulting density range recorded on the original film. An objective technique has been developed for determining the midrange exposure setting, E, based on the film H&D curve and the scene luminance range as a function of solar altitude.

H&D curves, resolution versus exposure curves, and the previously mentioned scene luminance ranges from Fig. 7 are shown in Figs. 9 and 10 for 3414 film processed in MX-619-1 developer. Observe that the optimal resolution for the film is located at the exposure required to produce a density of approximately 1.0. This exposure point is chosen as E since it corresponds to the exposure required for maximum resolution.

The scene luminances for each solar altitude and for the fore and aft camera conditions are converted to exposure values by Eq. 4. These exposure values for the scene luminance are shifted along the log E axis, locating the average scene luminance at the E point.*

Because the maximum exposure is reached at solar altitudes greater than terminator does not mean that photographs cannot be obtained. It merely intimates that at low sun angles the resolution will decline in accordance with the exposure-resolution functions and that in some situations the minimum luminances from those scenes will be exposed onto the toe portion of the H&D curves, resulting in a partial loss of information due to the compression of shadow detail.

*A shift to the left represents a decrease in exposure and a shift to the right an increase in exposure.

System Resolution

One of the oldest methods for describing the image forming properties of a camera system is its resolution or resolving power, i.e., its ability to record fine detail. The limitations of using resolving power for extended

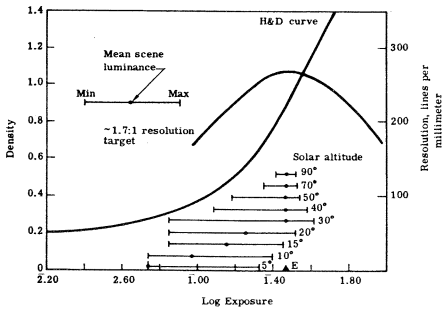

Fig. 9 — Forward looking camera analysis—H&D curve for 3414 film (MX-819-1 developer, AEI = 2.9, gamma = 1.96)

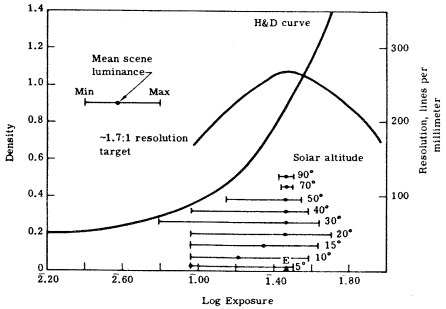

Fig. 10 — Aft looking camera analysis—H&D curve for 3414 film (MX-819-1 developer, AEI = 2.9, gamma = 1.96)

conclusions has long been recognized, especially since the introduction of the modulation transfer function (MTF) technique. However, in spite of its shortcomings, it still remains in common use, primarily because of its ease of implementation, its convenience, and its unique summary of numerous physical and subjective factors, and it is a useful bridge between the space and frequency domains.

Factors Affecting Resolution. The resolution of a camera system can be derived from the MTF of the optics and the aerial image modulation (AIM) or threshold curve of the emulsion. The optical MTF can be determined either mathematically or experimentally, and the AIM curves can be ascertained by determining the change in emulsion resolution as a function of test target modulation. If the two functions are plotted on a single graph with spatial frequency along the abscissa and modulation along the ordinate, the system resolution limit is defined where the two curves intersect.

In practice, the resolving power of the optical bar camera is altered by additional factors such as the camera filter, image movement, and target contrast. Each factor modifies the optical MTF by reducing the modulation, which in turn lowers the resolution. The choice of camera filter affects the chromatic aberrations by varying the width of the luminance bandpass. The optical bar lens is designed to be used with a Kodak Wratten 23A filter, which has a cutoff frequency at approximately 570 nm. If a filter having a wider bandpass and a cutoff frequency at 500 nm (i.e., Wratten 12) is used, the lens chromatic aberrations increase, causing a reduction in the MTF.

The transfer function for image motion has the form $\sin(\pi nx)/(\pi nx)$, where x is the displacement and goes to zero at a spatial frequency $n = 1/x$. The smear function is incorporated with the lens MTF by multiplying the two.

The intersection of the unmodified lens-smear MTF and the AIM curve indicates the resolution of a high contrast target. However, most aerial scenes are low contrast, ranging from approximately 1.6:1 to 10:1. The lens-smear MTF is therefore further degraded. The simplest procedure is to displace the MTF (plotted on logarithmic coordinates) downward so that it passes through zero frequency at the target modulation. In other words, a 2:1 target would lower the modulation to a value of 0.33.

When considering the optical bar parameters, each MTF was further degraded by a factor equal to a smear of 3.5 μm to simulate degradation effects of lens manufacture wavefront errors, defocus due to film dynamics, and thermal and pressure uncertainties. The 3.5 μm represents that smear which results in a predicted resolution of 145 l/mm with a Wratten 23A filter on Kodak 3404 film, a 2:1 contrast target, and a 2-msec exposure time.

Resolution Prediction. The predicted resolution as a function of the average scene luminance was determined by a two-step process: calculation of the exposure time and smear from Eq. 4 and then prediction of the resolution from the intersection of the film threshold curve with the appropriate smear-filter modified MTF's. A graphical example of this procedure is shown in Fig. 11 for a 2:1 scene contrast with a Petzval (no filter) MTF modified with several smear functions and a 3414 AIM curve.

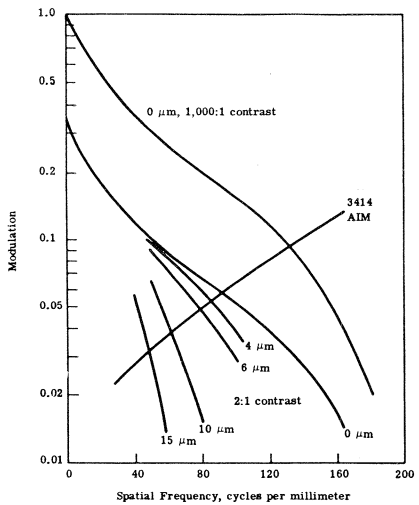

Fig. 11 — Optical bar Petzval lens MTF's and 3414 film AIM curve

The results of this analysis for 3414 film processed in MX-619-1 developer are shown in Figs. 12 and 13. These functions demonstrate the change in resolution and ground resolved distance as a function of average scene luminance and solar altitude from terminator.

The curves are calculated based on the previously described exposure point, for 2:1 and 10:1 scene contrasts, and for no filter, Wratten 12 filter, and Wratten 23A filter. The point where a maximum exposure of 0.0127 sec (0.3-in. slit) for 3414 film is reached is designated by the abrupt change in direction of the curves. The loss in resolution from that point to solar terminator photography is due to the reduced exposure.

Figs. 12 and 13 indicate that from a resolution standpoint, usable photography can be achieved at solar altitudes approaching the terminator. They do not, however, take into account the transfer of the scene luminance into density. As was pointed out, for 3414 film at low solar altitudes, some of the minimum luminances will be recorded on the toe region of the film characteristic curve, resulting in a partial loss of information. This condition may be especially obvious when utilizing either a Wratten 12 or 23A filter.

Disadvantages of Resolution as a Measure of Image Quality. The characterization of a system's image quality performance from a measure of resolution is misleading. The specification of a single resolution value for defining the optical bar system imaging capability is as meaningless as attempting to define the performance of a high fidelity electronic amplifier by its ability to reproduce sound waves of a single frequency. Resolution specification is easy, gives some indication of the capability of the system to record fine detail, and takes into account practically all parameters that make up the system specifications. Its advantages, however, lead to its major drawback. Since it is an all-encompassing measurement, it is often impossible to isolate the cause of system degradation with a single resolution determination.

Resolving power is not an indication of picture quality. The two most noticably conflict when using optics that possess unusual apertures or significant amounts of aberrations. Doubling the resolution does not necessarily result in doubling the system's information potential. It should always be kept in mind that the resolution is only a measure of the ability of a system to record a particular object of a particular configuration, contrast, and size.

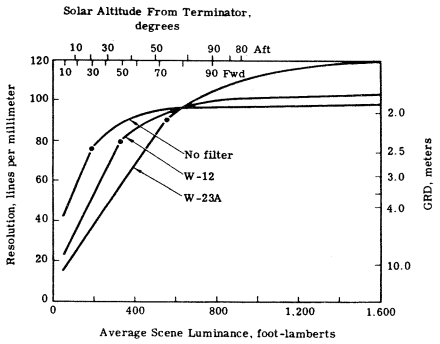

Fig. 12 — Resolution versus luminance for 3414 film at 2:1 contrast (MX-819-1 developer, exposure point = $\bar{1}.47$ = 0.296, 9% albedo)

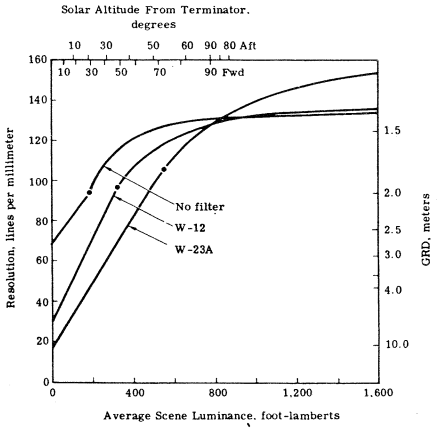

Fig. 13 — Resolution versus luminance for 3414 film at 10:1 contrast (MX-819-1 developer, exposure point = $\bar{1}.47$ = 0.296, 9% albedo)

Lunar Object Detection

Lunar object detection as a function of the mission film, its processing parameters, the exposure criteria, and the system transfer function is a complex problem that requires extensive study in order that the relationship of each to the others be completely understood and optimized.

It has been pointed out that resolution provides a far from adequate description of the optical bar image quality capability. It may give a superficial indication of the resolvability of lunar surface detail (ground resolved distance, GRD), but furnishes little or no information concerning lunar object detection.

Object Size Versus Ground Resolved Distance

Ground resolved distance is not directly applicable to the size of landing hazards for two reasons. First, the illuminated area of a hazard such as a boulder that is visible to the camera is much less than the actual size of the hazard, due to the geometry of the hazard. This is especially true at low solar elevations. Therefore, the nature of the hazard, the camera look angle, and the illumination conditions affect the apparent size of the object. Second, even though the projected illuminated area may be below the film-lens resolution limit, the point spread function may still be present as a photographic image. The hazard in this situation is not resolved, but is still detectable by means of the spread function.

The following example will illustrate. A prime objective of the optical bar photography is to analyze future Lunar Module landing sites for potential surface hazards. The minimum resolution requirement of approximately 100 l/mm was imposed on the system, since this resolution translates to a GRD of approximately 2 m. Assumptions were consequently made based on this GRD that a 2-m-diameter surface boulder could be resolved.

This is not entirely true. At low solar altitudes (7° to 20°) the system geometry involving the boulder's surface contour, the solar altitude, and the camera look angle restricts the visible size of the boulder to approximately 1 m, well below the resolution capability of the camera system. However, this does not mean that the 2-m boulder will be obscured on the film, but rather that it will be detected as a point spread function. An analysis of the point spread function created by this and other size boulders, and similarly small craters, will allow for more complete interpretation of the optical bar photography.

Definition of Tasks

The specific tasks accomplished in the study were:

1. Generation of photometric models of landing hazards such as boulders, steep slopes, etc., for various solar altitudes and fore and aft camera stereo angles. A generalized slope model will be developed so that the photometric model of any type of terrain feature may be synthesized.

2. Computer generation of the spread functions of the landing hazard photometric model on 3414 film, taking into account the various system parameters.

3. An analysis of the density distribution of the photometric model for various model sizes.

Photometric Model

A typical requirement of the optical bar camera is that it resolve a 2-m surface boulder. It is for this reason that such an object was chosen as the generalized photometric model, and it will be used as the basis for the detection study. Fig. 14 is a rendition of such an object showing the pertinent characteristics: (1) a diameter of 2 m, (2) a solar altitude of 22° 30', and (3) a camera look angle of 12° 30'. For illustration purposes the contours are represented as 20° slope increments.

If we assume that the surface material of the boulder conforms to the reflection characteristics described by Fedorets' photometric functions, the luminance distribution in the phase plane varies from 0 ft-L in the shadow to slightly greater than 234 ft-L at the surface contour perpendicular to the direction of the illumination vector. It is significant to note that although the boulder is 2 m in diameter, a sun angle of 22° 30' provides to a camera at a look angle of 12° 30' a visible portion of only approximately 0.8 m.

A complex luminance distribution of this model is used as input for the two-dimensional image processing computer program.

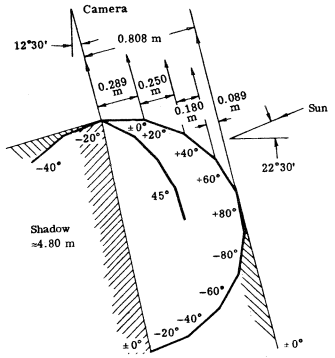

Solar Altitude, degrees	Luminance, foot-lamberts
0	93.6
20	164
40	201
60	234

Fig. 14 — Analysis of a 2-m boulder (solar altitude = 22° 30', forward looking camera, 9% albedo)

Two-Dimensional Computer Program

Two-dimensional image prediction by application of Fourier transform analysis has recently received wide attention, partly because of the increased flexibility and accuracy of the latest generation of general purpose digital computers. In the past, analysis of anything but elementary problems was severely restricted by lengthy computation time. However, a new method has been developed by Cooley and Tukey (Ref. 1) for the computation of a two-dimensional Fourier transform which drastically reduces the time. Recently, Lerman and Shannon (Ref. 2) demonstrated the feasibility of two-dimensional image prediction by incorporating the Cooley-Tukey algorithm along with other newly devised image processing techniques.

The luminance distribution of the lunar boulder is used as the input to the computer program. The input specifically consists of the luminance distribution calculated at the X-Y coordinates of a 128 by 128 matrix. The output can be all or any one of the three distributions: (1) a three-dimensional plot, (2) a contour plot, or (3) a laser beam recorder plot of the density distribution. These outputs are shown in Fig. 15. The three-dimensional plot is used primarily for visual examination and simply provides a "feel" of the surface characteristics. The contour plot indicates the luminance contours at 10% intervals of the maximum luminance value. Under certain circumstances, the contour plots are more useful than the three-dimensional plots, since exact values may be taken from this graph. The laser beam recorder image, like the three-dimensional image, should be used only as a visual reference. It does, however, provide a description of how the image would appear if it were recorded through an image system onto a light-sensitive material. Although no direct quantitative information can be obtained, the laser beam recorder image may, in fact, be most meaningful in terms of the visual impression of the predicted image density distribution.

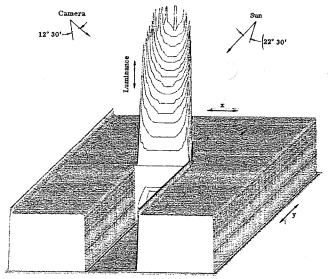

(a) Three-dimensional plot

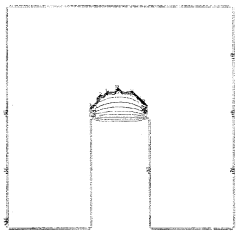

(b) Contour plot

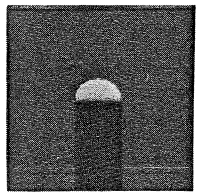

(c) Laser beam recorder plot

Fig. 15 — Luminance distribution of a 2-m boulder

The boulder size, a factor which will obviously affect the final image characteristics, is fixed by the sampling interval of the matrix pattern. The size can be changed, however, by merely altering a program constant. The physical parameters associated with the plots of Fig. 15 position the illuminance vector (sun) at the rear of the object at an angle of 22° 30' and the viewing vector (camera) at the front of the object at an angle of 12° 30'. The plateau of the graph represents the luminance of a flat lunar surface (0° slope), the trough is the shadow of the boulder cast on the surface (0 ft-L), and the central object is the luminance distribution of the boulder.

The object shown in Fig. 15 is now altered by factors associated with the system parameters. The available mathematical operations within the computer enable the program to be applied to the processing of images degraded by optical system aberrations (more specifically an optical transfer function), image motion, nonlinearities in the photographic process, and simulated grain noise. Although there are many other options available, such as atmospheric turbulence and defocus, it is the previously mentioned factors that are dealt with exclusively in this analysis.

The optical transfer function of the optical bar camera was mathematically derived, incorporating the specific parameters that will be utilized in the real flight situation. These factors include the aberrations of the optical system, the spectral sensitivity of the flight film, and the transmission of the optical system as altered by the camera filter. The input consists of a one-dimensional MTF which is converted to a two-dimensional function (Fig. 16) by rotating it 360° about the zero cycle spatial frequency.

The exposure distribution of the object, a 2-m-diameter boulder, degraded by the optical system is derived by computing the inverse transform of the object Fourier transform multiplied by the MTF. The three-dimensional, contour, and laser beam recorder plots of the distribution are shown in Fig. 17.

Image smear is introduced into the exposure distribution in accordance with the system parameters. This is accomplished by modifying the basic MTF with a sin X/X function of the camera motion and performing the identical

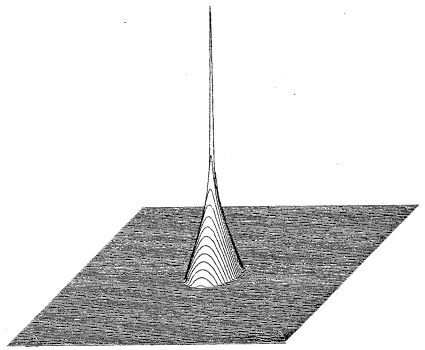

Fig. 16 — Optical transfer function of optical bar camera

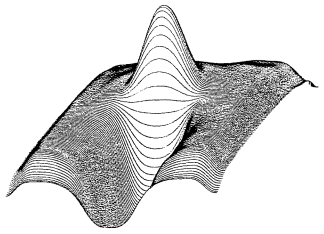

(a) Three-dimensional plot

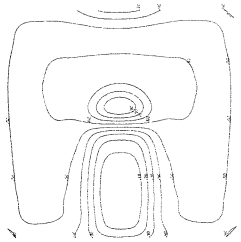

(b) Contour plot

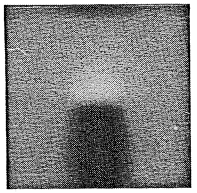

(c) Laser beam recorder plot

Fig. 17 — Exposure distribution of 2-m boulder modified by optical transfer function

multiplication between an object transform and the smear-modified MTF. Fig. 18 shows the effect of 10 μm of smear in the indicated direction.

The image, which is really an exposure distribution, is converted to a density distribution by interpolating the exposure values through a film H&D curve to density values. The difference between the exposure distribution (Fig. 17) and the density distribution (Fig. 19) is not startling, primarily because the interpolation was performed through the straight line portion of the H&D curve. If, however, the toe or shoulder region of the curve were used, e.g., in the case of an object having a wider luminance distribution, the suppression of exposure differences would show as a more pronounced factor.

The density distribution is actually further degraded by noise, a factor introduced by the inherent granularity of the film. The grain is simulated in the program by generating a Gaussian random noise array having a mean and standard deviation in accordance with the rms granularity function of the film. This simulated grain noise is then added to the density distribution; the results are shown in Fig. 20.

The above procedure for predicting the appearance of an image uses as an example a surface boulder 2 m in diameter. This size object, as was previously pointed out, is below the predicted resolution limit of the system, yet it obviously will be entirely possible to detect such an object, especially if the density distribution is known in advance.

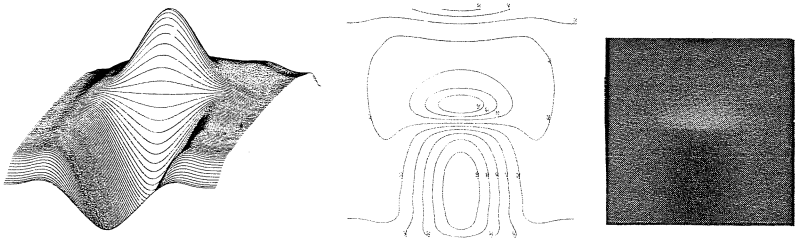

(a) Three-dimensional plot (b) Contour plot (c) Laser beam recorder plot

Fig. 18 — Exposure distribution modified with 10 μm of smear

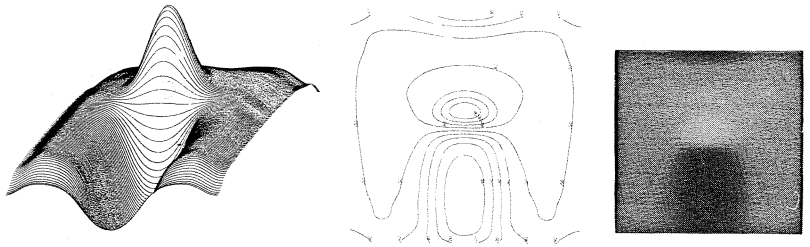

(a) Three-dimensional plot (b) Contour plot (c) Laser beam recorder plot

Fig. 19 — Density distribution of 2-m boulder modified by optical transfer function

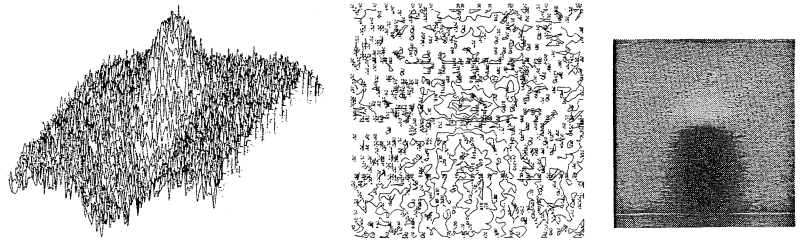

(a) Three-dimensional plot (b) Contour plot (c) Laser beam recorder plot

Fig. 20 — Density distribution incorporation film noise function

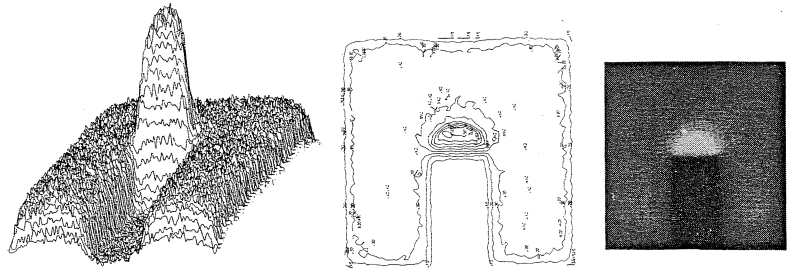

(a) Three-dimensional plot (b) Contour plot (c) Laser beam recorder plot

Fig. 21 — Density distribution of a 10-m boulder

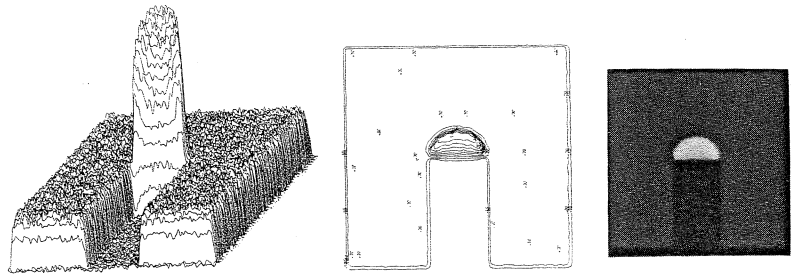

(a) Three-dimensional plot (b) Contour plot (c) Laser beam recorder plot

Fig. 22 — Density distribution of a 50-m boulder

Objects larger than 2 m in diameter can be investigated by simply changing a program constant, which in effect varies the sampling interval of the 128 by 128 luminance matrix. Naturally, as the object size increases, the image definition becomes increasingly pronounced. This effect can be seen from the density distributions of Figs. 21 and 22, which represent boulders having diameters of 10 and 50 m, respectively.

As was pointed out early in this paper, the lunar object detection study has only barely scratched the surface of what could be a valuable tool in photointerpretation of the lunar surface characteristics. Although at the outset the procedure appears complex and initial setup time extensive, the overall concept should not be abandoned.

Research into the field of computer prediction and manipulation of imagery is in its infancy. At present, many optical systems are specifically designed to be used with digital processing for image enhancements. Future reconnaissance systems may solely transmit digital data to ground stations where numerical techniques will be employed to enhance, reconstruct, or predict the image.

References

1. J. W. Cooley and J. W. Tukey, Math. Comp., 19:297 (1965).
2. S. H. Lerman and R. R. Shannon, Proceedings of the Computerized Imaging Techniques Seminar, 26-27 June 1967.

PART II

CAMERA EXPOSURE AND IMAGE QUALITY ANALYSIS

Introduction

In general, the Apollo optical bar camera produced photography of a quality level extremely close to its maximum dynamic capability. Establishing the image quality (detail) of the photography of terms of absolute resolution is, for the most part, an impossible task primarily because of the specific nature of this criterion and the obvious lack of either three-bar resolution targets or suitable edge objects on the surface of the moon. However, by examining the finest detail of the imagery and comparing it to images of known objects such as the LEM, Rover, and ALSEP we conclude that the system does detect objects that are significantly smaller than the predicted resolution limit. Image enhancement of this detail may increase the mensuration potential of the photography by providing additional confidence about the actual existence of questionable features.

The macroimage characteristics (i.e., the luminance distribution of the lunar surface and its associated density range as a function of solar altitude) are fundamental to the operation of the automatic exposure control (AEC) sensor, the surface luminance, and the exposure time setting. These parameters were controlled according to the pre-mission predictions. Analysis of the photography along with the associated telemetry data reveals a good correlation between the predicted and actual results, with a slight discrepancy indicating that the photography was approximately one-half stop overexposed. A portion of this discrepancy, however, was due to factors that were established subsequent to the publication of the predictions and relate to the processing of the photography.

This sequel to the original report is intended to examine the correlation between the predicted and actual results of the Apollo optical bar camera photography. It considers the anomolies associated with the camera performance, recommends adjustments that could be made prior to subsequent Apollo missions, and demonstrates the predicted benefits associated with such adjustments. The paper discusses the image quality of the photography by presenting samples of actual imagery and comparing them to ground truth obtained from surface photography taken by the astronauts.

Lunar Surface Luminance and Camera Exposure

The mean lunar surface luminance and luminance range as a function of solar altitude was calculated in part one and formed the basis, in conjunction with the predicted processing characteristics of 3414 flight film, for the exposure criteria for the optical bar camera. It was hypothesized that the AEC sensor mounted on the stereo gimbal of the camera would read the luminance of a surface area 10 by 30 mi, be influenced primarily by the luminance associated with the predominant terrain slope (the flat surface, 0° slope), and adjust the slit width accordingly. The proper exposure time was determined by shifting the log exposure range associated with the scene luminance range along the log exposure axis of the H&D curve of 3414 film, placing the mean predicted log exposure at the exposure required for maximum resolution. This located the minimum luminance in a region of the toe of the H&D curve where adequate separation of detail would occur and the maximum luminance on the straight line portion of the H&D curve.

Lunar Surface Luminance

The mean scene luminance as a function of solar altitude was calculated by measuring its density on the flight film, transforming that density to exposure using the sensitometry data associated with the processing characteristics of 3414 film, and applying the formula

$$B = \frac{E(f/no.)^2}{2.7tT} \qquad (1)$$

where E = exposure (meter-candle-seconds)
f/no. = f/number of Petzval lens = 3.5
t = exposure time for the particular frame (seconds)
T = lens transmission = 0.56

The frames measured are those that recorded the LEM landing sight covering a solar altitude range of 16°, 27°, 38°, and 50°. The results of the calculations are shown in Table 1. Also presented for comparison are the predicted luminance values, the measured luminances obtained from the AEC sensor telemetry data, and the adjusted luminance values. These adjusted values are given solely for comparative purposes and are derived by taking into account the difference in the 3414 H&D curve between the actual flight film processed by NASA and the curve used in predicting the luminance values.

Table 1 — Mean Luminance—0° Slope

Frame Number	Solar Altitude, degrees	Fore/Aft	Luminance			
			Predicted	Measured	Calculated	Adjusted
9370	16	Fore	160	100	260	222
9375	16	Aft	92	100	207	169
9377	16	Aft	92	100	141	114
9427	27	Fore	280	160	334	298
9430	27	Aft	194	190	376	335
9193	38	Fore	400	400	561	490
9798	38	Aft	270	300	478	418
9800	38	Aft	270	240	474	410
9809	50	Fore	510	400	609	532
9814	50	Aft	330	300	486	454

During the preflight prediction of luminance values (presented in part one), the fore and aft looking luminance values were calculated assuming the sun to be forward of the command module. During the mission, however, the sun was aft of the module, and therefore the comparison of the predicted and actual luminances must be made between the fore looking prediction and aft looking photography and vice versa.

There are several comparisons that can be made from Table 1, each leading to different conclusions concerning the correlation between the predicted and actual results, the operation of the AEC sensor, and the characteristics of the surface luminance.

Predicted Versus Measured Luminance. The comparison of the predicted to the measured luminances provides a measure of the correlation between the operation of the AEC sensor and the predicted luminances at the various solar altitudes. Note that in most instances the difference is less than 15%. The only significant discrepancy takes place at 27° solar altitude, where the sensor in the forward looking mode recorded a luminance lower than when in the aft looking mode. This situation, because of the geometry between the camera look angle and solar incidence angle, should not occur. The probable explanation for the discrepancy is that the field of view of the AEC in the forward mode may have covered a larger percentage of shadow area than in the aft mode, thereby reducing the measurement of the large area integrated luminances.

Predicted Versus Adjusted Luminance. The accuracy of the predicted luminance values can be determined from this comparison. The adjusted values are utilized because, as previously stated, they are corrected for the discrepancy between the actual and anticipated 3414 characteristic curves. The adjusted values are approximately 10 to 55% higher, with an average increase of 40%. The exact source of the

difference is not presently known; however, it is surmised that a portion is the result of a combination of items including, for example, the exact albedo at the landing sight* as well as some camera factors such as veiling glare that were not considered in the predictions. All of the discrepancies, however, are not explainable by these factors. Thus it is suspected that the predictions are lower than the actual surface luminance by approximately 50%.

Measured Versus Calculated Luminance. Assuming that the surface luminance is, in fact, higher than the predicted values, one would expect a correlation between the AEC measured and calculated luminance values. Table 1, however, shows the measured values to be lower, varying from approximately 125% at low solar altitudes to approximately 50% at higher altitudes. It is this range as a function of solar altitude that leads to the explanation of the inconsistency. The AEC sensor has a 10° by 30° field of view covering an area on the surface approximately 10 by 30 mi. It was hypothesized that the sensor would read the average surface luminance over that area and that the resultant measurement would closely represent the luminance associated with the predominant 0° surface slope. However, at the lower solar altitudes, a large portion of the sensor field of view contains shadow area. This has the effect of lowering the overall brightness measurement due to the luminance integration performed by the sensor. At increasingly higher solar altitudes, the percentage of shadow area within the field of view decreases, and the effective measurements more closely approximate the mean luminance. This phenomenon is observed in the measured to calculated luminance discrepancy.

It can therefore be concluded from this analysis that the mean scene luminance of the lunar surface is in the order of 50% higher than was predicted and measured by the AEC. This resulted in photography that was approximately one-half stop overexposed.

*The albedo used in the predicted calculations was 9%, the value considered as average for the entire lunar surface. It can range from 3 to 20%.

Luminance Range

The scene luminance range of the LEM landing site frames was calculated by the same procedure as was the mean luminance. The minimum and maximum densities containing just noticeable details were measured and incorporated into Eq. 1. The measurements of the shadow areas are excluded since they record as base plus fog density and would make the determination of the luminance range meaningless. The results of this analysis are shown along with the predicted ranges in Figs. 1 and 2 for the forward and aft looking camera conditions. These figures indicate the log exposure ranges as a function of solar altitude and the log exposure calculation of the mean luminance. These log exposures are projected through the H&D curve to establish the recorded density associated with each luminance condition.

Recall that the exposure criterion for the predicted scene luminance was established such that the mean scene luminance was exposed onto the H&D curve at the log exposure required for peak resolution. This represents a log exposure of $\bar{1}.50$ and is the reason that the mean log exposures for the predicted mean luminance are located at that point. The mean luminances determined from the actual photography, however, vary about the $\bar{1}.70$ log exposure or are approximately 0.2 higher than optimum.

This overexposure, further substantiated by the previous discussions, affects the overall quality of the photography in two ways. First, it results in a longer than necessary exposure time, the results of which will be discussed subsequently, and second, it records the scene luminances at a density higher than optimum for maximum information. The latter consequence increases the chance for highlight information to be recorded in the shoulder region of the characteristic curve, and even more important, records the scene information at high densities where some reduction in image quality due to higher granularity is likely to occur.

Overexposure

The AEC light sensor mounted on the stereo gimbal relates the degree of ground scene brightness to the sensor and controls the light falling on the film by adjusting a variable slit width mechanism. This slit width mechanism

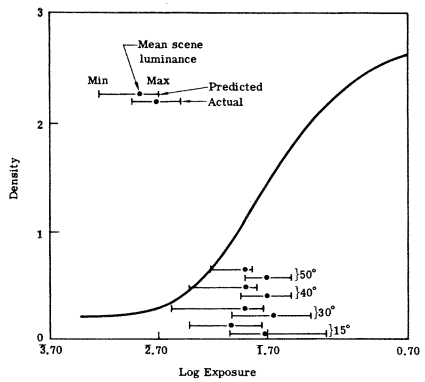

Fig. 1 — Predicted versus actual exposure points for scene luminances at various solar altitudes in forward looking mode (Fultron processor, MX-819-1 developer)

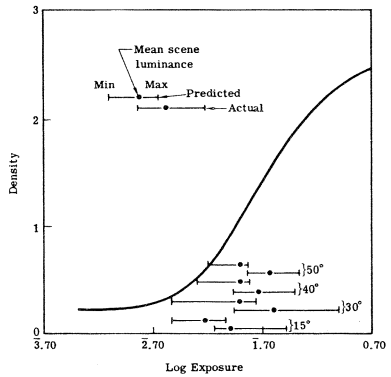

Fig. 2 — Predicted versus actual exposure points for scene luminances at various solar altitudes in aft looking mode (Fultron processor, MX-819-1 developer)

is commanded to open and close in accordance with the varying scene luminance. A switch, externally mounted to the camera, permits the selection of one of four exposure settings, three representing different mean exposure values for type 3414 film and one representing a selected mean exposure value for type 3400 film. These settings provide the correction factor necessary to obtain the appropriate slit width for the exposure values they represent.

The three 3414 switch positions provide correction factors necessary to obtain the following three slit width openings:

1. Selected mean exposure value: $\bar{1}.50$
2. Selected mean exposure value plus overexposure: $\bar{1}.70$
3. Selected mean exposure value minus underexposure: $\bar{1}.30$.

The switch position selected for the Apollo 15 mission was the mean exposure value of $\bar{1}.50$. This presumably located the predicted mean luminance at the log exposure corresponding to the peak resolution.

From the analysis it was determined that the actual mean luminance log exposure is approximately $\bar{1}.70$ or 0.20 log above the optimum setting. Therefore, switching to the $\bar{1}.30$ position would properly correct the exposure at the various solar altitudes. The results of this maneuver are shown in Figs. 3 and 4.

The log exposure ranges of the landing site photography for the fore and aft looking frames are shown for the various solar altitudes. The lower range is the actual measurement and the upper range is the shift that would be experienced if the exposure switch on the camera were changed from $\bar{1}.50$ to $\bar{1}.30$. It is clear that a decrease in exposure would locate the mean luminance log exposure at $\bar{1}.50$ and in no way jeopardize the proper recording of the shadow detail by exposing it on the toe of the H&D curve. Furthermore, it would reduce the possibility of overexposure at the subsolar point where the slit is approaching its minimum width, reduce the overall density of the photography, thus increasing its image quality because of the lower granularity, and allow the AEC sensor to maintain control over the slit to a lower solar altitude. It would, moreover, not in any way affect terminator photography, since the slit would be completely open and no longer under automatic control.

An increase in resolution would also be realized. One of the primary degradation factors affecting the image quality of the photog-

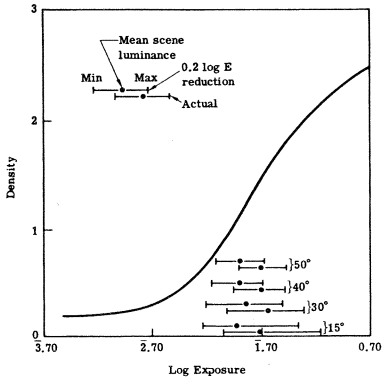

Fig. 3 — Result of 0.20 reduction in log exposure for forward looking mode (Fultron processor, MX-819-1 developer, speed = 3.88, gamma = 1.74)

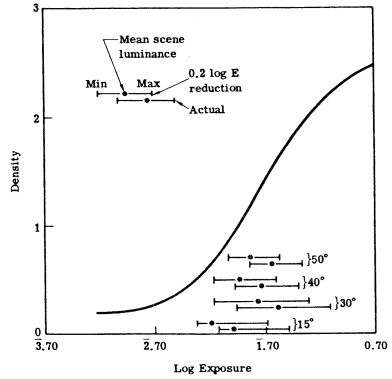

Fig. 4 — Result of 0.20 reduction in log exposure for aft looking mode (Fultron processor, MX-819-1 developer, speed = 3.88, gamma = 1.74)

raphy is the presence of smear. Smear increases with exposure time. Therefore, as the exposure time is reduced, the image motion is likewise reduced, resulting in higher resolution and a lower ground resolved distance (GRD).

The effect of a switch adjustment on these factors is shown in Fig. 5. Observe that the

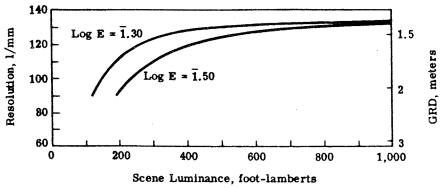

Fig. 5 — Increase in resolution as a function of log exposure setting (3414 film, no filter, 10:1 target contrast, 9% albedo, MX-819-1 developer)

increased resolution is most pronounced at the lower luminance levels where the resolution increases from 90 to 110 l/mm, resulting in a GRD improvement of approximately 20%.

In conclusion, it has been shown that the predicted scene luminances as a function of solar altitude are very close to those actually measured off the flight film. The minor descrepancy due to higher than predicted scene luminance levels resulted in an overall overexposure of approximately one-half stop, not sufficient to degrade the photographic image quality below design goals. The AEC sensor measurements were influenced by the extensive deep shadow areas of the lunar scene, predominantly at the lower solar altitudes, thereby preventing it from compensating for the higher than predicted scene luminance. Adjustments can easily be made to compensate for the overexposure, resulting in an increase in overall image quality and a 20% improvement in GRD.

Resolution, Detection, and Recognition

Visual analysis methods must be employed in analyzing the image quality of the Apollo 15 lunar photography since the nature of the surface detail and the absence of ground targets rule out the various mathematical approaches such as modulation transfer function determination from edge trace measurements. The image quality of an aerial photographic image can be qualitatively analyzed in terms of resolution, detection, and recognition. In each case visual processes are used to make judgments of quality. Thus the result of the analysis is dependent on the various physiological processes associated with an individual observer and is, therefore, prone to considerable variation between observers.

It is important to understand the differences between resolution, detection, and recognition, both in the manner in which each is implemented and in the ramifications attached to the conclusions, since each provides a totally different conclusion concerning the true quality of the imagery. Mr. Paul Rosenburg has recently described the three techniques in detail (Ref. 1). Since a broad based discussion concerning resolution and detection was presented in part one in association with the image quality predictions and lunar object detection study, it will suffice here merely to summarize Mr. Rosenburg's discussion.

Resolution

Resolution is the most common criterion for judging the imaging capability of an optical system. The measurement, generally expressed in lines per millimeter, is a quantitative expression of a visual analysis of the imagery of a specific target configuration usually consisting of a pattern of regularly placed bars and spaces. Since there are no such targets on the lunar surface, it is obvious that judging the quality of the Apollo 15 imagery using resolution predictions or GRD calculations will provide little correlation to the actual results.

Detection

Detection requires only the visual perception of the presence or absence of an object. The object size can be well below the predicted resolution limit of the system, but if its brightness is sufficiently different from that of its background, the object will record on the photographic emulsion as a point or line spread function. The density distribution of the spread function is determined by a complex relationship between the film modulation transfer function characteristic and the brightness of the object. Two objects of different dimensions both still well below the resolution of the system and having the same overall luminance will have identical sized spread functions but their density distributions will vary widely.

Detectability can provide a more realistic measure of the imaging capability of a camera system than resolution. Although the true nature of the object may not be identified from a spread function image, it does, nevertheless, furnish information concerning the existence of meaningful surface features. For example, a lunar rock may be well below the predicted GRD of the Apollo 15 photography but still be detectable as a potential LM landing hazard.

Recognition

Recognition requires the visual characterization of the nature of an object, e.g., an observer must be able to identify the image of a rock as a rock. The size of an object required for recognition is thus much larger than that required for resolution or detection, especially in the absence of clues from the environment. There is no established numerical scale that can define the recognition capability of a camera system primarily because the analysis is almost purely subjective in nature.

Thus a signal can be detected without being resolved or recognized, it can be resolved and detected without being recognized, it can be detected and recognized without being resolved, but it cannot be resolved and recognized without being detected. It is the first case, being detected without being resolved or recognized, that we will mainly deal with here to attempt to define the operational image quality of the Apollo 15 optical bar photography.

Image Quality

Qualitative judgments based on visual inspection of the imagery appears to be the only technique with the potential of supplying meaningful performance data. However, observing unfamiliar lunar detail on the panoramic photography must result in a degree of uncertainty unless a comparison can be made with some sort of ground truth.

The following examples of actual panoramic camera photography indicate its image quality by showing the detectability of particular lunar detail accompanied by substantiating ground truth either in the form of surface photography taken by the astronauts or post-mission data supplied by NASA. It should be noted that these examples were generated from duplicate positives printed from the original negatives and therefore do not represent the ultimate quality, and they are presented in both a negative and positive format in order to minimize the number of printing generations to retain maximum detail.

It should also be noted that this analysis is not intended to demonstrate the capability of the panoramic photography to locate objects similar in size to the ALSEP or even to substantiate their existence. It is obvious that there are numerous areas that could be misinterpreted in the absence of substantiating evidence. It is presented only to point out the detection capability of the imagery.

LM Landing Site

The first example, the LM landing site, as photographed on rev. 27, is shown in Fig. 6. The LM, measuring 5 m in diameter, is clearly evident. Parking next to the LM is the rover. Located approximately 350 feet to the west-northwest is the ALSEP central station (CS) along with the cold cathode gauge (CCG) experiment, the lunar surface magnetometer (LSM) experiment, and the laser ranging retro-reflector (LRRR) experiment. The surface disturbance between the LM and ALSEP was produced by the astronauts during deployment.

Because of the uncertainty in detecting objects that are well below the predicted resolution, photography taken before and after deployment of the rover and ALSEP was compared. This comparison is shown in Fig. 7. The before photograph is from rev. 16 taken at a solar altitude of approximately 15°, and the after

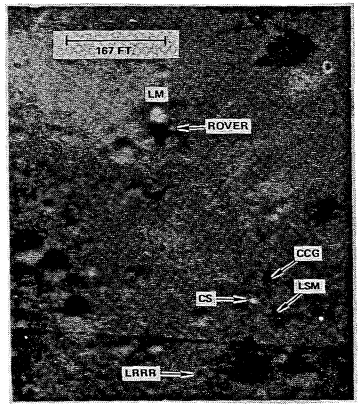

Fig. 6 — Panoramic photograph of LM landing site (rev. 27, positive)

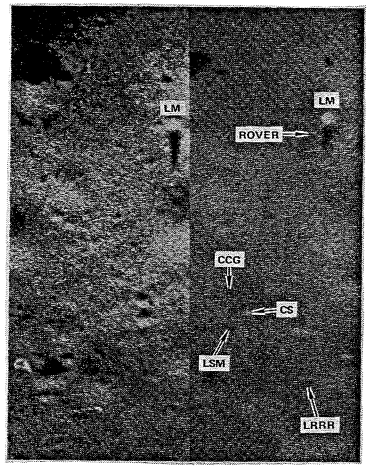

Fig. 7 — Comparison of LM landing site before and after deployment of rover and ALSEP (positive)

photograph is from rev. 27, taken at a solar altitude of approximately 27°. Note the absence of natural features at the rover and ALSEP central station sites. The latter is particularly conspicuous due to the highly reflective nature of the object. There is, however, a question concerning the location of the CCG, LRRR, and LSM stations since it appears that these areas could be caused by natural lunar features.

The location of the CCG, LRRR, and LSM experiments is substantiated by Fig. 8 (Ref. 2), which was derived from a photograph taken from the LM during ascent. Note the location of the experiments as compared to those indicated in Fig. 9, which is an enlargement of the pan photograph from rev. 27. Of the three, the LRRR is the most obscure, probably because of the intentional lack of activity while setting up the experiment to minimize the dust problem, but there is still evidence of activity in the area.

Rover Tracks and Rock

The second example concerns the detection of rover tracks produced during EVA 1 between stations 1 and 2 at the elbow of Hadley Rille and a 2-m rock photographed by James Irwin at station 2.

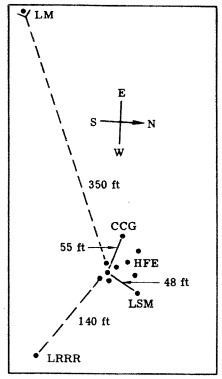

Fig. 8 — Map of ALSEP placement derived from photograph taken from LM during ascent

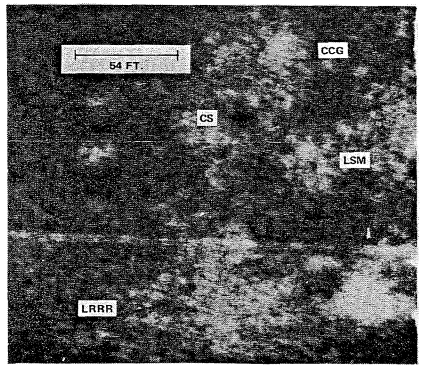

Fig. 9 — Panoramic photograph of ALSEP deployment (rev. 27, negative)

A NASA map showing the route taken by the rover during EVA 1 is shown in Fig. 10 (Ref. 2). The rover traveled from the LM to the edge of Hadley Rille, along the Rille to station 1 at the east side of Elbow Crater, made a loop to station 2 located between Elbow and St. George Craters, where the rock was photographed, and back to the LM. An analysis of a photograph (Fig. 11) of the area encompassing the indicated locations of stations 1 and 2 taken by the pan camera during rev. 27 (after EVA 1) revealed

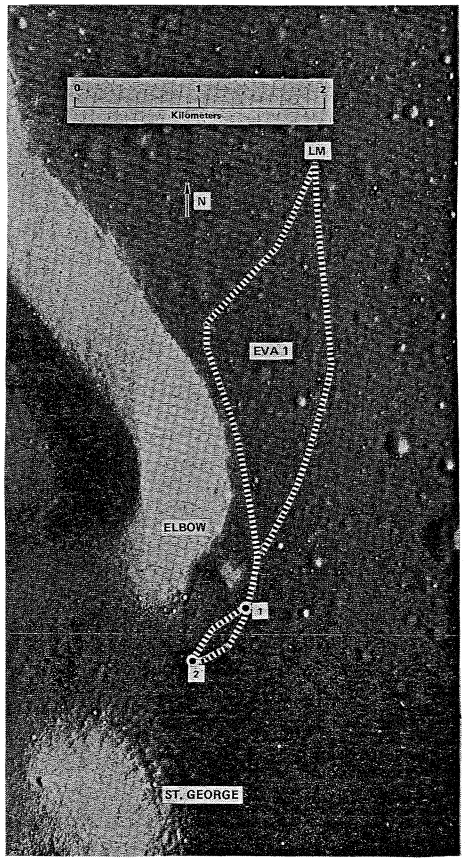

Fig. 10 — Route of rover during EVA 1 (negative)

what seem to be rover tracks. These tracks emerge from a location at the west side of Elbow Crater, proceed in the direction of station 2, and then appear to return to station 1 in a loop. The location of station 2 is different from that shown on the map, being slightly west and north, and the location of station 1, according to the rover tracks, is on the west rather than east edge of Elbow Crater. In spite of these differences, there seems to be enough evidence to indicate that these are rover tracks.

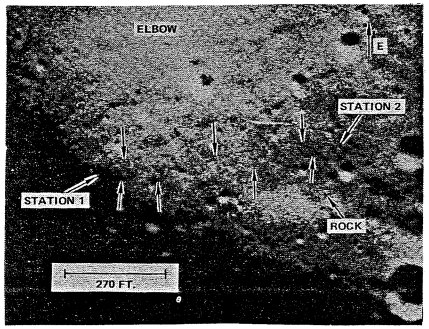

Fig. 11 — Panoramic photograph of rover tracks west of Elbow Crater (rev. 27, positive)

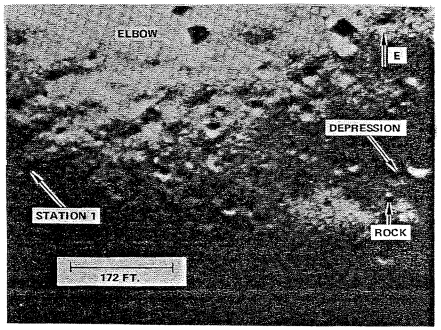

Fig. 13 — Panoramic photograph of lunar rock and depression at station 2 (rev. 16, positive)

The rock photographed by James Irwin at station 2 is shown in Fig. 12. Comparison with the size of the rover would indicate it to be approximately 2 m in diameter. It is located to the west of a slight depression in the surface, which can be seen in the lower left corner of the photograph. The rock is only barely visible in the pan photography taken during rev. 27 because of the higher solar altitude, but is very evident in the rev. 16 photography (Fig. 13), where the solar altitude is approximately 15°.

There is some question as to whether the rock observed on the pan photography is the same one pictured in the surface photography. There are four clues to substantiate that they are the same. First, there is a depression detected in the pan photography whose location corresponds to the one shown in Fig. 12. Second, the rover tracks emanating from station 1 at the west side of Elbow Crater appear to proceed to and terminate at the proposed location of station 2. Third, close examination of the surrounding area reveals a total lack of surface features that meet the conditions established by the ground truth. Fourth, the rock measures approximately two-fifths the size of the 5-m LM.

The lunar object detection study presented in part one discussed the appearance of a 2-m rock at a solar altitude of 22°30'. This analysis was performed using computer image processing techniques to degrade the expected luminance distribution of a 2-m rock with the various camera components, i.e., lens MTF, film MTF, H&D curve characteristics, and film granularity. Fig. 14 shows the pan camera rock enlarged to a size permitting direct comparison with the computer-generated 2-m rock prediction. Note the similarity between the two illustrations. Both rocks are recorded as a modified point spread function with a definite separation at the interface between the edge of the rock and the shadow area.

Photo courtesy of NASA

Fig. 12 — Composite photograph taken by James Irwin at station 2

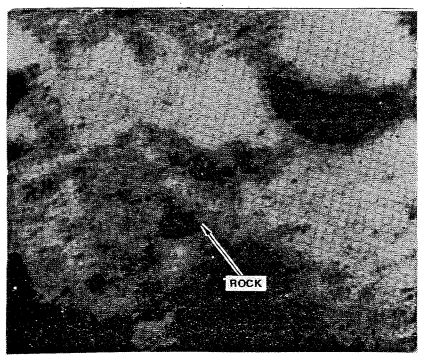

(a) Panoramic photograph (rev. 16, negative)

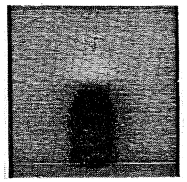

(b) Computer prediction

Fig. 14 — Comparison of panoramic photograph of lunar rock and computer predicted appearance of a 2-m rock

The characteristic density grading at the edges of the shadow shows up in both instances. The only pronounced discrepancy is in the granularity, with the actual rock showing a higher effect. To a great extent this is due to the numerous printing stages necessary to enlarge the rock to a size suitable for comparison. If the original negative image of the rock could be analyzed, it is expected that such a discrepancy would not exist.

Summary

In summary, the overall analysis of the Apollo 15 pan camera photography leads to the following conclusions. The camera's performance level was better than anticipated, and exceeded the manufacturer's design goals. The photography was approximately one-half stop overexposed, especially at the lower solar altitudes, and correction would result in a 15 to 20% improvement in GRD. It is possible to detect lunar surface objects, both man-made and natural, that are far smaller than the predicted resolution limit of the system.

References

1. P. Rosenburg, "Resolution, Detectability and Recognizability," Photogrammetric Engineering, 37(12) (Dec 1971).
2. Apollo 15 Mission Report, MSC-05161, Manned Spacecraft Center, Houston, Texas, Dec 1971.

THE AUTHOR

WILLIAM C. KINNEY joined the Optical Systems Division of Itek Corporation, Lexington, Massachusetts, six years ago; and directed the program to determine the film, filter, and exposure combinations for the Itek Apollo optical bar panoramic camera. His work with Itek has included the direction of research toward defining the image quality of color materials, and the investigation of techniques for increasing the information content of high altitude aerial photography. Mr. Kinney's background includes research into all types of film processing techniques and research into all types of film processing techniques and research in development of a mordant blank film. Mr. Kinney's B.S. is in Photographic Science (1964) from the Rochester Institute of Technology.